Supporting Information

Mayers et al. 10.1073/pnas.1302918110

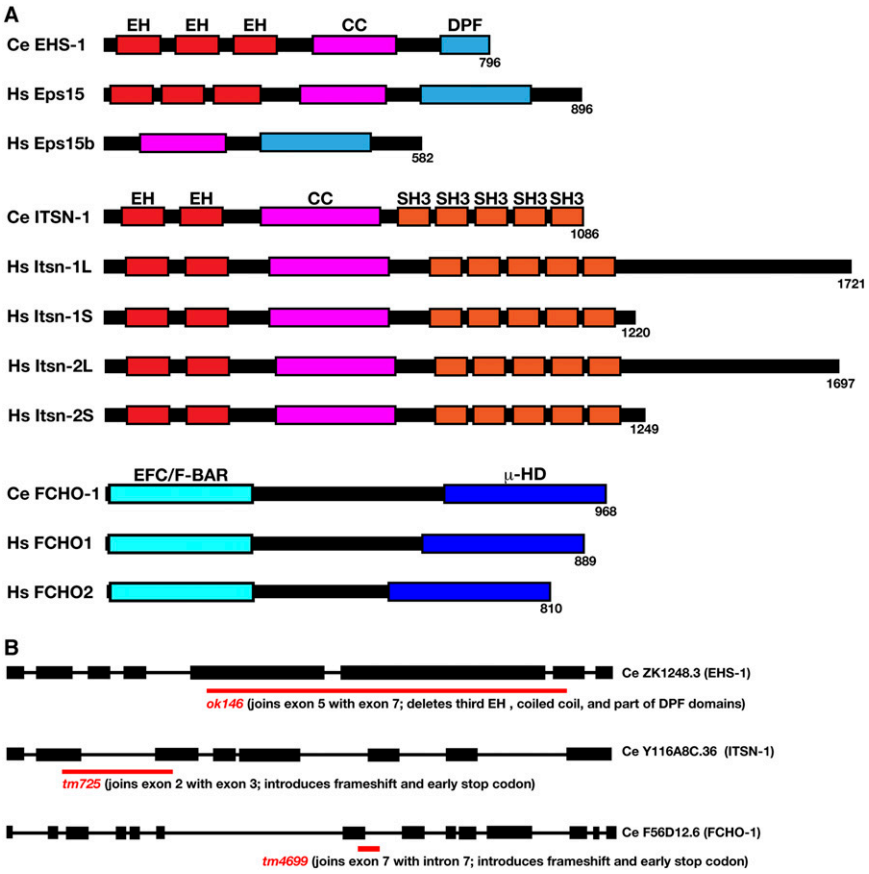

Fig. S1. The domain organization of human and *Caenorhabditis elegans* Eps15, intersectin, and FCHO proteins are conserved. (*A*) Cartoons depicting the domain architecture of the *C. elegans* and human isoforms of Eps15, intersectin, and FCHO proteins. CC, coiled-coil domain; DPF, Aspartic acid-proline-phenylalanine rich domain; EFC/F-BAR, Extended FCH homology domain/FCH-BAR domain; EH, Eps15-homology domain; μ-HD, mu homology domain; SH3, Src homology 3 domain. (*B*) Predicted gene models for *ehs-1*, *itsn-1*, and *fcho-1*. Exons and introns are shown to scale. Deletion mutations (highlighted in red) and a brief description of the predicted effect of each are provided.

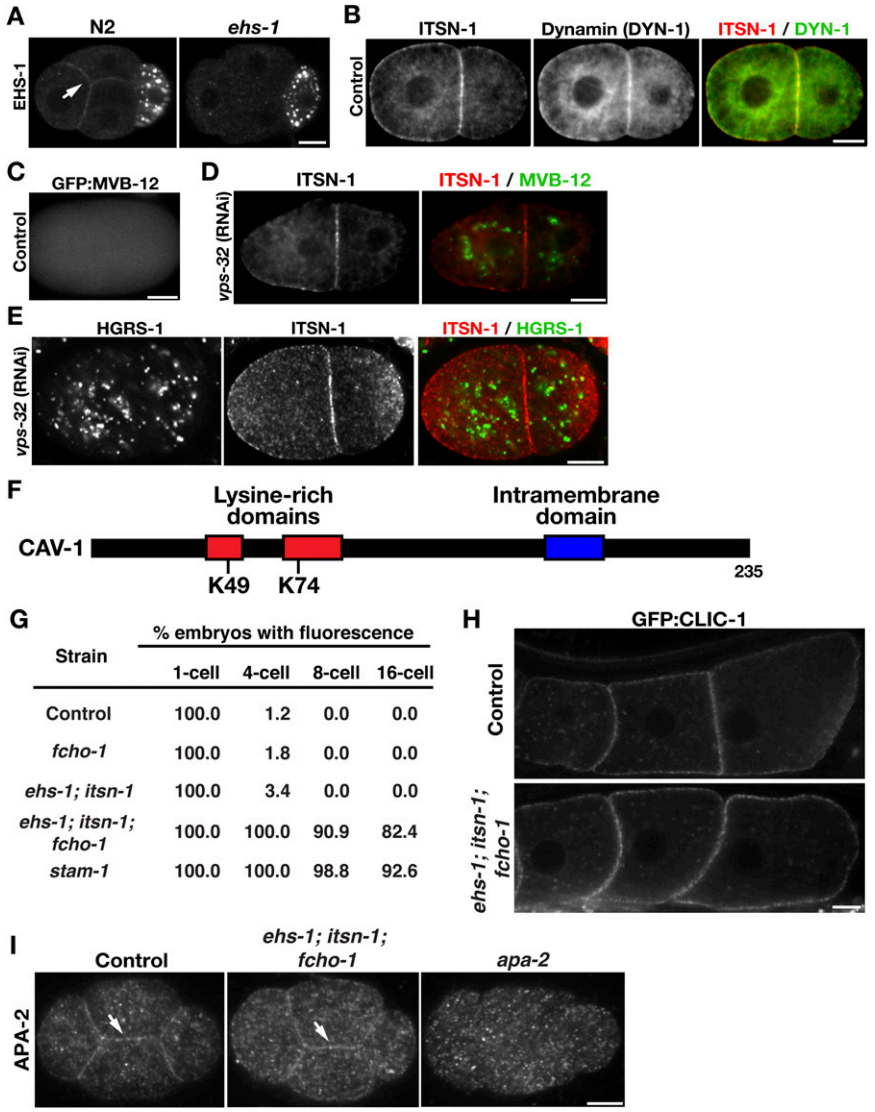

Fig. S2. The components of the FEI complex (FCHO-1, EHS-1, and ITSN-1) localize specifically to the plasma membrane and do not accumulate on endosomes. (*A*) Four cell stage control and *ehs-1* mutant embryos were fixed and stained by using antibodies directed against EHS-1 and visualized by using swept-field confocal optics. An arrow highlights the plasma membrane localization of EHS-1. Nonspecific staining in the P1 cell is present in both control and *ehs-1* mutant embryos. (*B–D*) Two-cell stage control (*B* and *C*) or VPS-32 depleted (*D*) embryos expressing GFP-DYN-1 (*B*) or GFP-MVB-12 (*C* and *D*) were fixed and stained by using antibodies directed against ITSN-1 and GFP (*B* and *D*) or imaged live (*C*). Embryos were imaged by using swept-field confocal optics. (*E*) Two cell stage, VPS-32 depleted embryos were fixed and stained by using antibodies directed against ITSN-1 and HGRS-1. Embryos were imaged by using swept-field confocal optics. (*F*) Cartoon depicting the domain architecture of a *C. elegans* isoform of caveolin-1 (CAV-1). Two lysine residues in the amino-terminal cytosolic region of CAV-1 were identified as potential sites for ubiquitin modification (K49 and K74), based on mass spectrometry analysis of a CAV-1 immunoprecipitate (isolated specifically from an embryo extract). For this experiment, we immunoprecipitated GFP:CAV-1 (in the presence of *N*-ethylmaleimide) by using GFP antibodies that were coupled to Protein A agarose. Following a low pH elution, CAV-1 was TCA precipitated, washed extensively with acetone, and dried by using vacuum centrifugation. The pellet was solubilized, and disulfide bonds were reduced. Free thiols were then alkylated, and the sample was digested sequentially with Endoproteinase Lys-C and trypsin. The reaction was quenched after 12 h, and samples were pressure loaded onto a fused silica capillary desalting column, which was placed inline with a Hewlett Packard Agilent 1100 Quaternary Pump and analyzed by using a customized four-step separation method (90, 120, 120, and 150 min, respectively). A distal 2.5-kV spray voltage was applied to elute the peptides from the microcapillary column. This applied voltage caused the peptides to directly electrospray into a linear trap quadrupole (LTQ) two-dimensional ion trap mass spectrometer. For each step of the multidimensional cycle, one full-scan mass spectrum (400–2,000 *m/z*) occurred followed by five data-dependent MS/MS spectra at a 35% normalized collision energy. Spectra were searched against a recent version of the *C. elegans* protein database by using the SEQUEST algorithm. The search was set up to consider a possible modification of +114 on lysines, which corresponds to the two glycine residues from ubiquitin that remain attached to a target lysine after trypsinization. The program DTASelect was used to filter peptide identifications and manually validate spectra that correspond to putative ubiquitin attachment sites. (*G*) Table illustrating the defects observed in GFP:CAV-1 degradation a variety of strains, as indicated. Embryos containing at least 15% of the GFP fluorescence intensity observed immediately following ovulation were counted as being fluorescent ($n = 15$ animals each). (*H*) Control and *fcho-1*; *ehs-1*; *itsn-1* triple mutant animals expressing a GFP fusion to clathrin light chain (CLIC-1) were imaged by using swept-field confocal optics. Loss of all components of the FEI complex fails to alter the enrichment of clathrin on the plasma membrane of oocytes in the *C. elegans* germ line. (*I*) Control, *fcho-1*; *ehs-1*; *itsn-1* triple mutant, and *apa-2* single mutant embryos were fixed and stained by using an antibody directed against endogenous APA-2 (the alpha subunit of the AP-2 complex) and imaged by using swept-field confocal optics. Loss of all components of the FEI complex fails to alter the enrichment of AP-2 on the plasma membrane of embryos. Intracellular fluorescence observed in *apa-2* mutant embryos reflects nonspecific staining. (Scale bars: 10 μm.)

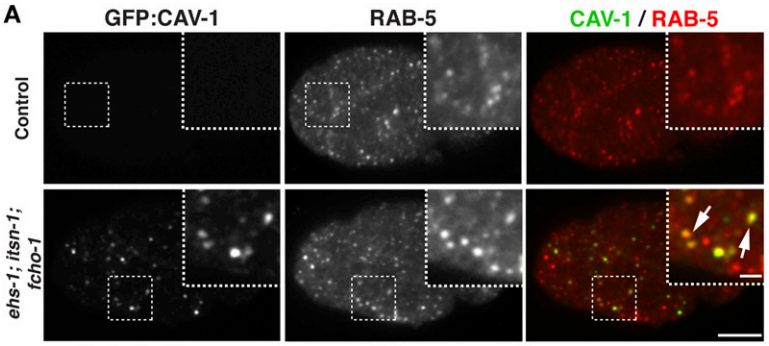

B

	CAV-1 internalization		% Viability (n>200 each)	
	N2	*ehs-1; itsn-1; fcho-1*	N2	*ehs-1; itsn-1; fcho-1*
Mock	+	+	100%	55%
unc-41 (RNAi)	+	+	91%	55%
unc-11 (RNAi)	+	+	100%	75%
apa-2 (RNAi)	+	+	100%	28%
dab-2 (RNAi)	+	+	100%	37%
num-1 (RNAi)	+	+	100%	62%
epn-1 (RNAi)	+	-	91%	40%

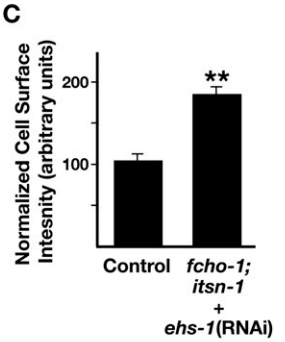

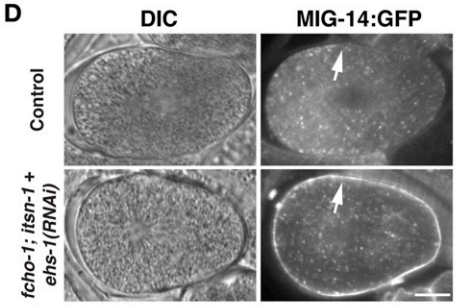

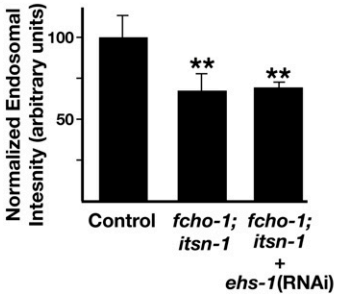

Fig. S3. Inhibition of FEI complex function affects endocytosis in a cargo-selective fashion. (*A*) Four cell stage control and *ehs-1;itsn-1;fcho-1* triple mutant animals expressing GFP:CAV-1 were fixed and staining by using antibodies directed against GFP and RAB-5. Embryos were imaged by using swept-field confocal optics. *Inset* showing a 2× zoom of the boxed regions is provided. Arrows highlight endosomes that exhibit both CAV-1 and RAB-5 staining. (*B*) Table indicating the impact of various double-stranded RNAs (dsRNAs) on the viability (through early larval development) and internalization rate of GFP-tagged CAV-1 in control and *fcho-1*; *ehs-1*; *itsn-1* triple mutant embryos. (*C*) Bar graph showing the relative fluorescence intensities (following background subtraction) of cell surface MIG-14:GFP during metaphase of the first embryonic division in control and *fcho-1;itsn-1* double mutant animals (treated with dsRNA targeting EHS-1). **, statistically significant difference compared with control ($P < 0.01$). (*D*) Control and *fcho-1;itsn-1* double mutant animals expressing MIG-14:GFP were analyzed in utero by using DIC and swept-field confocal optics. The mutant animals were treated with dsRNA targeting EHS-1 to better mimic the genetic perturbation of *ehs-1;itsn-1;fcho-1* triple mutant animals. The embryos shown were tracked until metaphase of the first embryonic division to highlight differences in MIG-14:GFP localization under each condition. We failed to observe any increase in MIG-14:GFP accumulation on endosomes following inhibition of the FEI complex, regardless of embryonic stage. (*E*) Bar graph showing the relative fluorescence intensities (following background subtraction) of endosomal compartments containing MIG-14:GFP during metaphase of the first embryonic division in control and *fcho-1;itsn-1* double mutant animals (with or without additional treatment with dsRNA targeting EHS-1). **, statistically significant difference compared with control ($P < 0.01$). (Scale bars: *A* and *D*, 10 μm; *Inset*, 2.5 μm.)

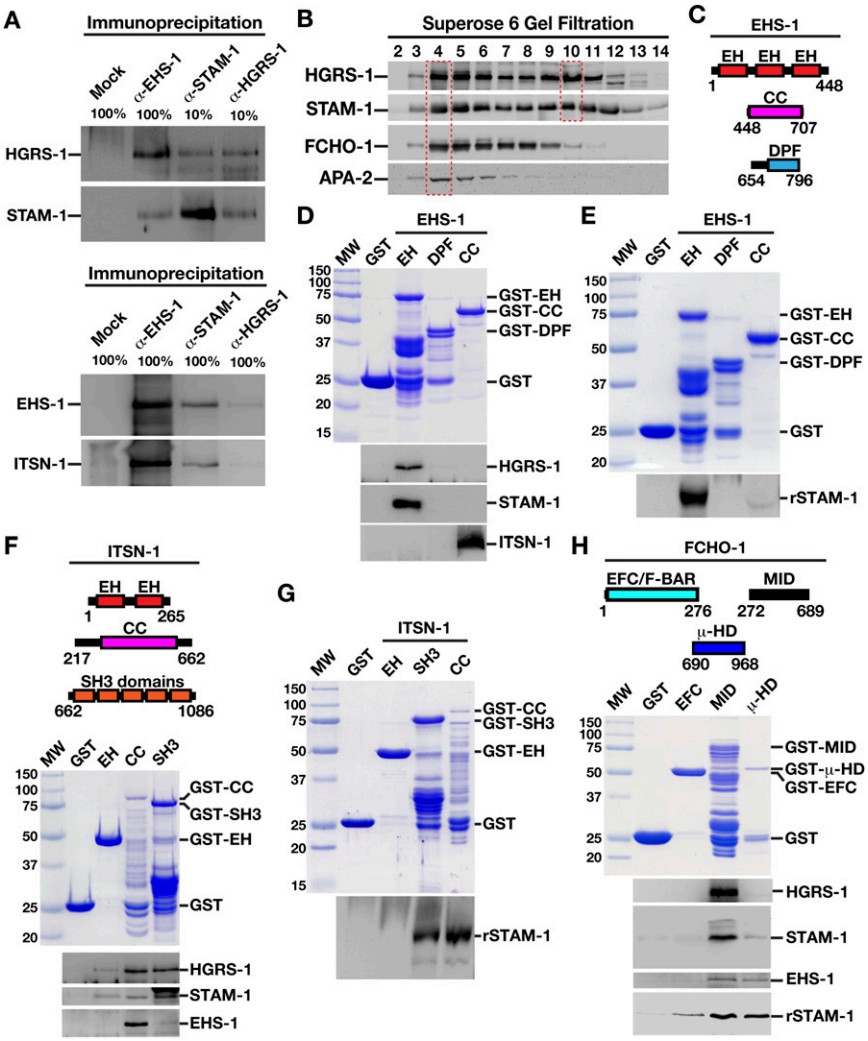

Fig. S4. Components of the FEI complex bind to ESCRT-0. (*A*) Antibodies directed against GFP (Mock), EHS-1, STAM, and HGRS-1 were used to immunoprecipitate each protein and interacting partners from *C. elegans* embryo extracts. Immunoprecipitates were immunoblotted for the presence of HGRS-1, STAM, EHS-1, and ITSN-1. (*B*) An embryo extract was separated by gel filtration chromatography, and eluted fractions were immunoblotted by using antibodies directed against HGRS-1, STAM-1, FCHO-1, and APA-2. Based on densitometry measurements, peak fractions were identified for each protein (boxed regions). (*C*) Cartoon diagrams highlighting the various regions of EHS-1 that were purified as GST fusion proteins for interaction studies. (*D–H*) GST and various domains of EHS-1, ITSN-1, and FCHO-1 (see cartoons) fused to GST were immobilized on glutathione agarose beads and incubated with *C. elegans* embryo extracts or recombinant STAM-1 (rSTAM-1). The eluted fractions from the beads were immunoblotted for the presence of HGRS-1, STAM-1 (or rSTAM-1), EHS-1, and ITSN-1.

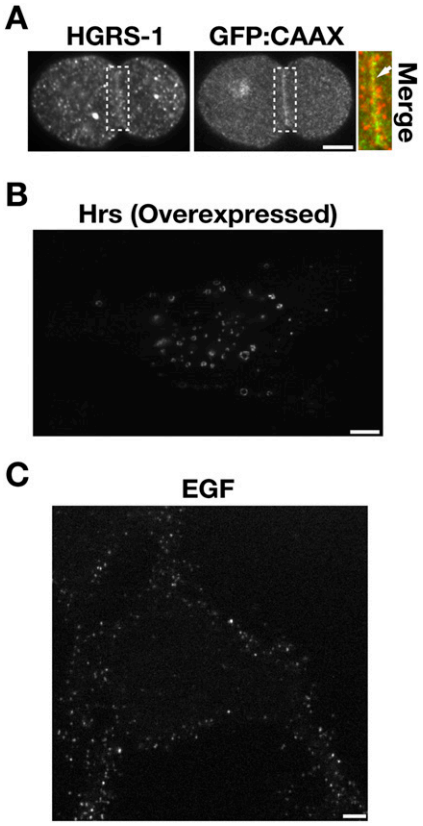

Fig. S5. ESCRT-0 is recruited to the plasma membrane. (*A*) Embryos expressing a GFP fusion to a CAAX box (GFP:CAAX) were stained by using antibodies directed against endogenous HGRS-1 and GFP and imaged by using swept-field confocal optics. A 1.6× zoom of the boxed region indicated is shown as a color overlay (*Right*). (*B*) HeLa cells overexpressing YFP-tagged Hrs were imaged by using swept-field confocal optics. (*C*) HeLa cells pretreated with dynasore were pulse labeled with EGF (directly labeled with Alexa-647) for 2 min, followed by fixation and imaging by using swept-field confocal optics. A medial section of a representative cell is shown. Under these conditions, EGF is restricted to the cell surface. (Scale bars: 10 μm.)

Table S1. Viability of embryos lacking one or more endocytic adaptor proteins

	N2		*fcho-1*		*ehs-1*; *itsn-1*		*ehs-1*; *itsn-1*; *fcho-1*	
APA-2 depletion	–	+	–	+	–	+	–	+
Embryos analyzed, *n*	529	1,096	645	791	982	1,507	400	779
Viability, %	100	100	93	92	100	97	55	28

Table S2. Identification of EHS-1, ITSN-1, STAM-1, and HGRS-1 interacting partners using immunoprecipitation followed by solution mass spectrometry

		Sequence coverage, %				
C. elegans gene	Human homolog(s)	EHS-1 (IP)	ITSN-1 (IP)	STAM-1 (IP)	HGRS-1 (IP)	Predicted size, kDa
stam-1 (C34G6.7)	STAM (ESCRT-0)	12.0	9.8	42.0	35.4	50.8
hgrs-1 (C07G1.5)	Hrs (ESCRT-0)	4.1	4.8	35.0	22.1	83.3
chc-1 (T20G5.1)	Clathrin Heavy Chain	27.2	9.8	25.5	26.1	191.5
clic-1 (T05B11.3)	Clathrin Light Chain	5.2	15.5	24.8	4.6	24.4
itsn-1 (Y116A8C.36)	Intersectin	59.1	26.1	30.1	4.8	120.5
ehs-1 (ZK1248.3)	Eps15	50.7	28.0	27.8	3.7	86.6
fcho-1 (F56D12.6)	FCHO1/2	12.0	13.7	15.6	4.3	108.5
apa-2 (T20B5.1)	AP-2α subunit	3.4	13.2	8.1	8.9	104.2
apb-1 (Y71H2B.10)	AP-2β subunit	4.3	12.3	11.6	13.2	105.2
dpy-23 (R160.1)	AP-2μ subunit	—	21.1	5.9	4.1	50.3
tsg-101 (C09G12.9)	Tsg101 (ESCRT-I)	—	—	13.9	14.5	46.2

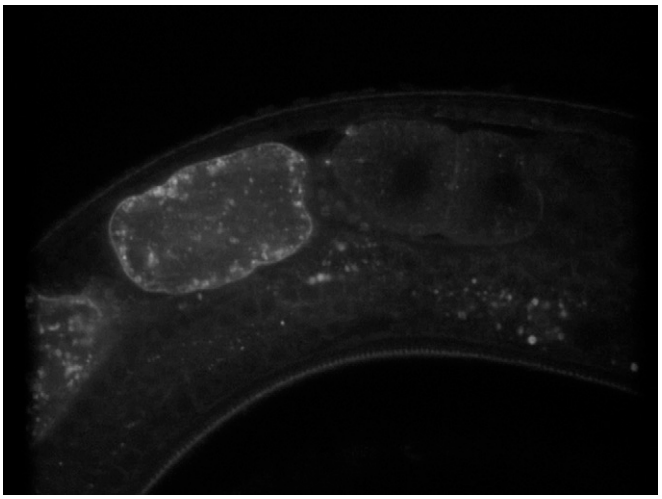

Movie S1. CAV-1 dynamics during ovulation in control animals. Live animals expressing GFP:CAV-1 were immobilized on 10% agarose pads in the presence of 0.1-μm diameter polystyrene microspheres. Time-lapse imaging was conducted by using swept-field confocal microscopy. Images were acquired at 20-s intervals.

Movie S1

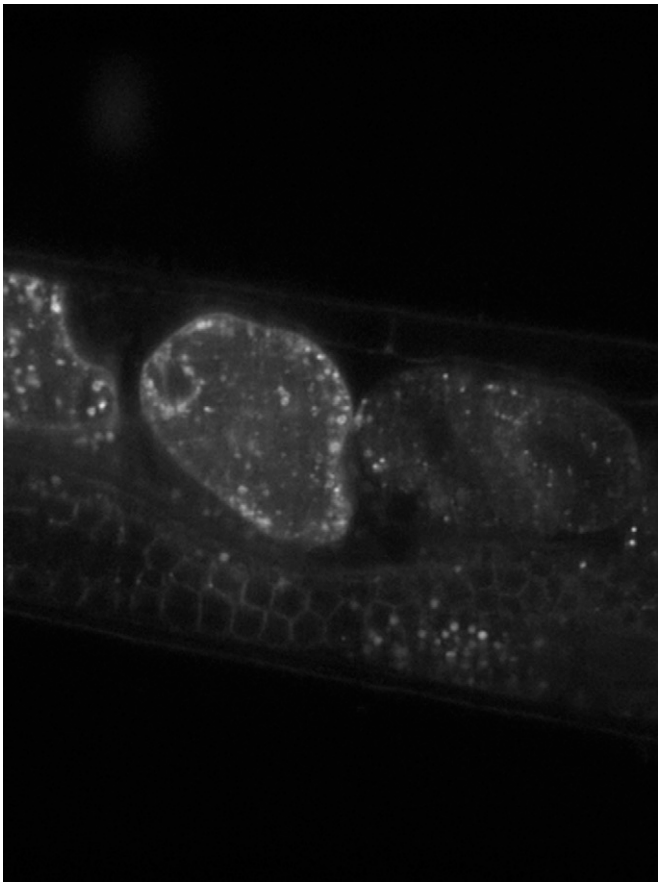

Movie S2. CAV-1 dynamics during ovulation in *fcho-1*; *ehs-1*; *itsn-1* triple mutant animals. Animals lacking all components of the FEI complex and expressing GFP:CAV-1 were immobilized on 10% agarose pads in the presence of 0.1-μm diameter polystyrene microspheres. Time-lapse imaging was conducted by using swept-field confocal microscopy. Images were acquired at 20-s intervals.

Movie S2

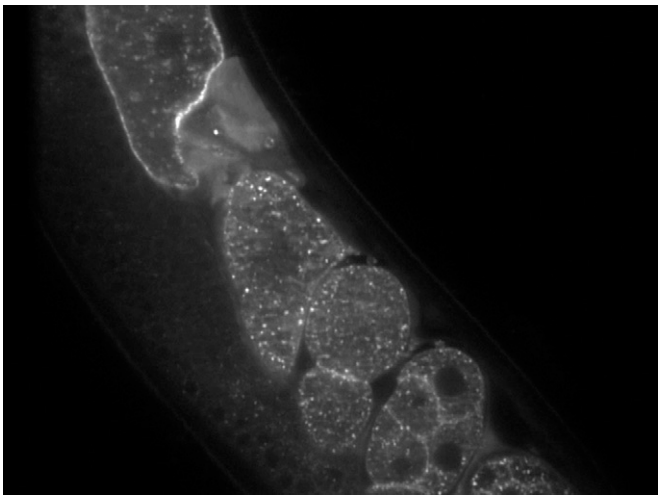

Movie S3. MIG-14 dynamics during ovulation in control animals. Live animals expressing GFP:MIG-14 were immobilized on 10% agarose pads in the presence of 0.1-μm diameter polystyrene microspheres. Time-lapse imaging was conducted by using swept-field confocal microscopy. Images were acquired at 20-s intervals.

Movie S3

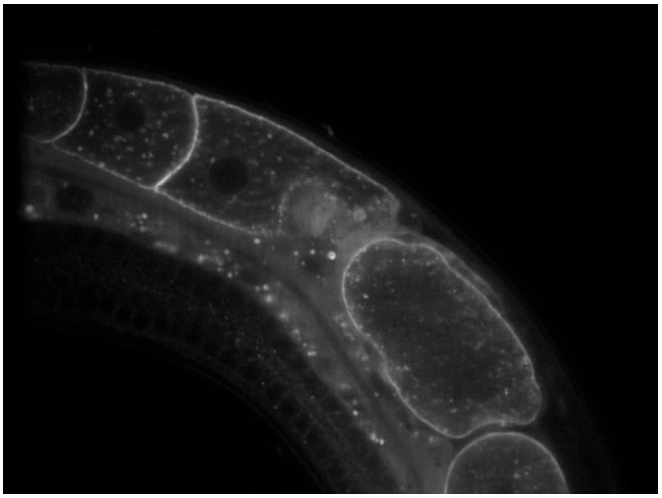

Movie S4. MIG-14 dynamics during ovulation in animals lacking all components of the FEI complex. Double mutant animals (*fcho-1*; *itsn-1*) expressing GFP: MIG-14 were depleted of EHS-1 by using RNAi and immobilized on 10% agarose pads in the presence of 0.1-μm diameter polystyrene microspheres. Time-lapse imaging was conducted by using swept-field confocal microscopy. Images were acquired at 20-s intervals.

Movie S4